

EXTRACTING 21CM SIGNAL BY FREQUENCY AND ANGULAR FILTERING

QIZHI HUANG,^{1,2,3} FENGQUAN WU,¹ REZA ANSARI,³ AND XUELEI CHEN^{1,2,4}

¹*Key Laboratory of Computational Astrophysics, National Astronomical Observatories, Chinese Academy of Sciences, Beijing 100101, China*

²*School of Astronomy and Space Science, University of Chinese Academy of Sciences, Beijing 100049, China*

³*Université Paris-Sud, LAL, UMR 8607, F-91898 Orsay Cedex, France & CNRS/IN2P3, F-91405 Orsay, France*

⁴*Center for High Energy Physics, Peking University, Beijing 100871, China*

ABSTRACT

Extracting the neutral hydrogen (HI) signal is a great challenge for cosmological 21cm experiments, both the astrophysical foregrounds and the receiver noise are typically several orders of magnitude greater than the 21cm signal. However, the different properties of the 21cm signal, foreground, and noise can be exploited to separate these components. The foregrounds are generally smooth or correlated over the frequency space along a line of sight (l.o.s.), while both the 21cm signal and the noise varies stochastically along the same l.o.s. The foreground can be removed by filtering out the smooth component in the frequency space. The receiver noise is basically uncorrelated for observations at different times, hence for surveys they are also uncorrelated in the different directions, while the 21cm signal which traces the large scale structure are correlated up to certain scales. In this exercise, we apply Wiener filters in frequency and angular space, to extract the 21cm signals. We found that the method works well. The inaccurate knowledge about beam could degrade the reconstruction, but the overall result is still good, showing that the method is fairly robust.

1. INTRODUCTION

The neutral hydrogen 21cm line of is one of the most promising tools to study the observable universe. Tomographic observation of the redshifted 21cm line could be used to reveal the evolution of the intergalactic medium (IGM) throughout the Epoch of Reionization (EoR) (Madau et al. 1997; Ciardi & Madau 2003), to map out the large scale structure and constrain the cosmological parameters including the dark energy equation of state (Chang et al. 2008; Mao et al. 2008). In principle, it could even probe the cosmic dark age (Loeb & Zaldarriaga 2004). Comparing with the cosmic microwave background (CMB), which images the Universe at the last scattering surface during the epoch of recombination, one advantage of the redshifted 21cm tomography signal as a cosmological probe is that it provides three dimensional (3D) map of the Universe at different redshifts, giving more information and also showing how the Universe evolved.

In recent years, a number of experiments set the 21cm observation as one of their main scientific goals, for example the experiment with existing telescopes such as the GBT (the Green Bank Telescope; Chang et al. 2010; Masui et al. 2013; Switzer et al. 2013), GMRT (the Giant Metrewave Radio Telescope; Paciga et al. 2011), and telescopes newly built or being built, such as the 21CMA (Zheng et al. 2016), Tianlai (Chen 2012), BINGO (BAO from Integrated Neutral Gas Observations; Battye et al. 2013), LOFAR (the LOw-Frequency Array; van Haarlem et al. 2013), MWA (the Murchison Widefield Array; Tingay et al. 2013), PAPER (the Precision Array for Probing the Epoch of Re-ionization; Parsons et al. 2010), CHIME (the Canadian Hydrogen Intensity Mapping Experiment; Bandura et al. 2014), HERA (the Hydrogen Epoch of Reionization Array; DeBoer et al. 2017), FAST (Nan et al. 2011) and the SKA (Huynh & Lazio 2013), etc.

Although the redshifted 21cm line can provide a large amounts of information for cosmology, its detection is difficult. The cosmological 21cm signal whose brightness temperature ~ 0.14 mK at redshift $z \sim 0.8$ (Chang et al. 2010; Masui et al. 2013) is highly contaminated by the foreground emissions whose brightness temperatures are 4–5 orders of magnitude higher (de Oliveira-Costa et al. 2008; Liu & Tegmark 2012). The foregrounds at low frequency include primarily the Galactic synchrotron emission which is originated from the cosmic ray electrons moving in the Galactic magnetic field, the Galactic free-free emission which is produced by free electrons scattering off ions without being captured, extragalactic radio sources such as radio-loud galaxies and quasars (Shaver et al. 1999; Jelić et al. 2008). Additionally, the observa-

tion are also affected by the radio frequency interference (RFI) and propagation effects in the ionosphere.

Removing the foregrounds has been a big challenge in the redshifted 21cm experiments, and a number of methods have been proposed and developed. The general idea is to exploit the different properties of foregrounds and cosmological 21cm signal. Along one line of sight (LoS), the cosmological 21cm signal varies with redshift or frequency randomly, while the the astrophysical foregrounds vary smoothly. The foreground can in principle be removed by light-of-sight fitting (Wang et al. 2006; Glezer et al. 2008) or by cross-correlating different frequency bins data (Santos et al. 2005). More recently, blind or semi-blind methods such as the Singular Value Decomposition (SVD) method (Paciga et al. 2011; Masui et al. 2013), Robust Principle Component Analysis (Zuo et al. 2018), and Independent Component Analysis (Chapman et al. 2012; Wolz et al. 2014), are applied.

In this paper, we introduce a simple and fast method which is based on the Wiener filter to extract the 21cm signal. The Wiener filter has been widely used in signal processing, especially for removing noise in time series or images. We use a simulation to demonstrate our method.

The rest of this paper is structured as follows. In Sec. 2, we describe the Wiener filter method in general, and also describe the set up of our simulation. In Sec. 3, we apply the method to the simulated data, and present the results we obtained. Finally, we discuss a number of relevant issues in the data processing and concludes in Sec. 4.

2. METHOD

In a HI intensity mapping survey experiment, the observed sky emission is a mixture of the 21cm signal, noise and foregrounds, to extract the cosmologically interesting 21cm signal, their different statistical properties are used to separate them. On the relevant scale, the cosmological 21cm signal varies stochastically, as the signal strength at each frequency corresponds to the emission of a specific redshift, and on large scales the density at each different position are independent to each other (though there is correlation to some degree). By comparison, the foreground varies smoothly in frequency space, so it could in principle be distinguished from the 21cm line. In addition to the sky signals, the electronic circuit of the receiver also generate noise. After band-pass calibration, the noise could be approximated as zero-mean white noise. Based on their different properties, it is in possible, at least in principle, to extract the 21cm signal from the much stronger foregrounds and noise.

In an actual radio telescope, the data would be first pre-processed to remove bad data (e.g. those with hardware malfunction or radio frequency interference), calibrated, re-binned in frequency and time resolution, rearranged in predefined order, then used to form images cubes with two angular dimension and one frequency dimension. These steps will depend on the particular telescope in question, e.g. the data of a single dish telescope would be processed very differently from the data of an interferometer array. Here, we will deal the data processing after these steps. We shall assume that an image cube have been obtained through these steps.

Below we make the 21cm signal extraction in two steps. In the first step, we filter the data along each l.o.s, to remove the foreground component by using their different properties. As a result, the foreground data could be significantly suppressed, while the 21cm signal and the thermal noise is kept. In the second step, we filtering the data in the 2D angular space, to remove the randomly fluctuating noise signal, while keeping the more stable and consistent 21cm signal.

2.1. Wiener Filter

We assume that in an experiment the observational data \mathbf{y} is linearly related to \mathbf{x} , the physical quantity we try to measure,

$$\mathbf{y} = \mathbf{A}\mathbf{x} + \mathbf{n} \quad (1)$$

where \mathbf{A} is the response matrix of the system, and \mathbf{n} is random noise. We use boldface letter to denote vectors and matrices, and T denotes matrix or vector transpose (we assume the data are real numbers here). The covariance matrices for the signal and noise are $\mathbf{S} = \langle \mathbf{x}\mathbf{x}^T \rangle$, $\mathbf{N} = \langle \mathbf{n}\mathbf{n}^T \rangle$ respectively. If \mathbf{S} and \mathbf{N} are known, an unbiased estimate of the signal can be obtained by applying a Wiener filter \mathbf{W} to the data (Tegmark 1997),

$$\hat{\mathbf{x}} = \mathbf{W}\mathbf{y} \equiv \mathbf{S}\mathbf{A}^T [\mathbf{A}\mathbf{S}\mathbf{A}^T + \mathbf{N}]^{-1} \mathbf{y} \quad (2)$$

The Wiener filter is optimal in the sense that it minimizes the variance of the estimator

$$V = \langle (\mathbf{x} - \hat{\mathbf{x}})(\mathbf{x}^T - \hat{\mathbf{x}}^T) \rangle$$

2.2. Simulation Setup

As the signal extraction utilizes our prior knowledge or expectation of the 21cm signal, foreground and noise, the optimal filter depends on the statistics of them, so the property of the filter also depends on the particular problem. Here we describe the basic setup we use in this exercise.

We consider the the mid-redshift experiment aimed at detecting the baryon acoustic oscillation (BAO) signal of the large scale structure, such as the ongoing survey projects on GBT (Masui et al. 2013; Switzer et al. 2013), and dedicated experiments such as Tianlai (Chen 2012; Xu et al. 2015; Zhang et al. 2016a,b), CHIME (Bandura et al. 2014), BINGO (Dickinson 2014) and HIRAX (Newburgh et al. 2016). For such projects, the (synthetic) aperture is $50 \sim 100$ m. Below, we shall consider a fiducial frequency of 800 MHz ($z = 0.7755$) and 100 m aperture, the corresponding full width half maximum (FWHM) resolution of 0.25° .

We generate the 21cm signal as follow. We adopt the Planck 2015 (Planck Collaboration et al. 2016) best fit cosmological parameters for our fiducial model. For $z = 0.7755$ the corresponding comoving angular diameter distance is $D_A = 1068.95 \text{ Mpc } h^{-1}$. We consider a frequency resolution of 0.1 MHz, the corresponding to a comoving radial distance interval of $\Delta D_c = 0.43 \text{ Mpc } h^{-1}$ at this redshift. For our 21cm simulation, we generate an image cube with 200^3 voxels, which is convenient for computation. Then the frequency interval is 20 MHz, i.e. $790 \sim 810$ MHz. The corresponding angular size per pixel is $\Delta\theta = \Delta D_c / D_A = 0.023^\circ$, smaller than the beam FWHM, which is good as our computation precision would not be affected by too large pixel sizes. The whole box has an angular area of $4.6^\circ \times 4.6^\circ$. The volume of the corresponding 3D box in real space is $V = L^3 = (86 \text{ Mpc } h^{-1})^3$.

We assume a thermal noise with $\sigma_n = 200$ mK per voxel, which is $\sim 10^3$ times of the 21cm fluctuation ~ 0.2 mK in our frequency (redshift) range. Note that the beam area is about 10^2 times of the pixel area, so if the pixel noise is independent of each other, this corresponds to a noise level of $\sigma_T = 20$ mK per beam. Note that using the measurement equation

$$\sigma_T \sim \frac{T_{\text{sys}}}{\eta\sqrt{\Delta\nu t}}, \quad (3)$$

where $\eta < 1$ is the efficiency of the system, and take $\Delta\nu = 0.1$ MHz. If the system is stable with a typical system temperature of $T_{\text{sys}} = 20 \text{ K} \sim 100 \text{ K}$, and the noise is thermal, this level of noise can be achieved with a few minutes integration time. However, in the real telescopes there might be a noise floor of non-thermal origin preventing the noise reaching the low thermal value given by Eq. 3 no matter how long the integration time, so the actual noise might be higher.

Assuming the neutral hydrogen evolution is linear on the relevant scales, the dark matter power spectrum is shown in Fig. 1. We then generate random density distribution in the simulation box according to the power

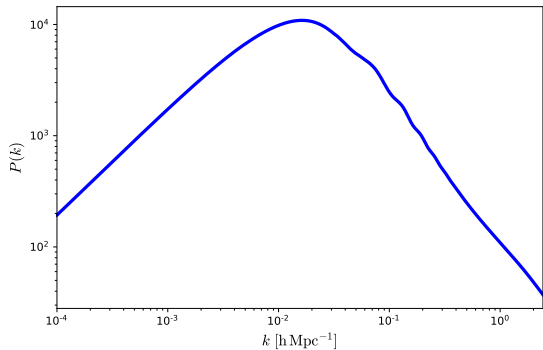


Figure 1. Power spectrum of dark matter at $z = 0.7755$ (with non-linear correction).

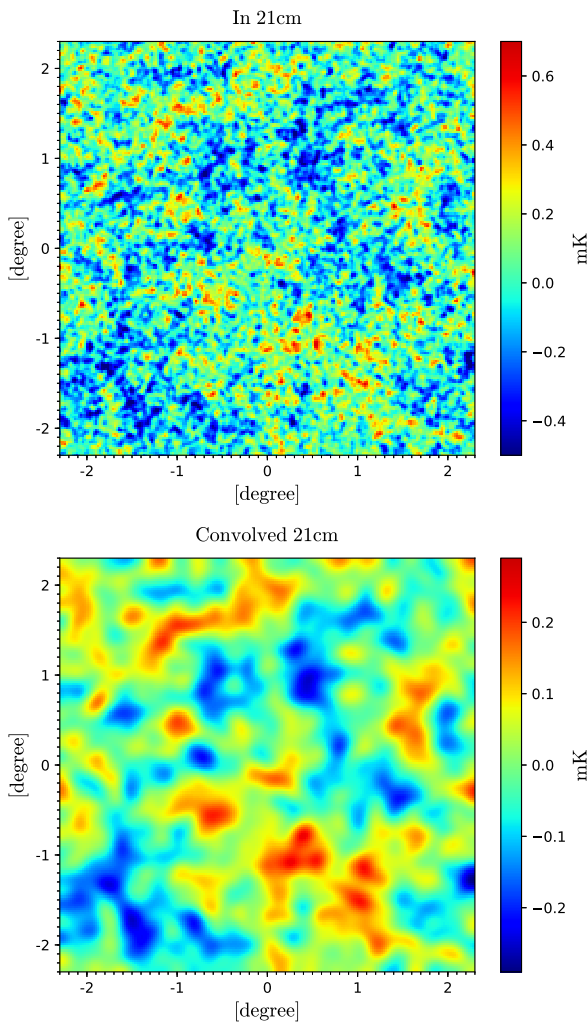


Figure 2. Top: the simulated 21cm signal at 800 MHz; bottom: the 21cm signal convolved with a FWHM 0.25° Gaussian beam.

spectrum. Adopting an HI bias of $b_{\text{HI}} = 0.70$ and HI density ratio $\Omega_{\text{HI}} = 6.6 \times 10^{-4}$ Chang et al. (2010); Masui et al. (2013), the average brightness temperature of 21cm signal around $z \sim 0.8$ is given by

$$\bar{T}_{21} \approx 0.284 \left(\frac{\Omega_{\text{HI}}}{10^{-3}} \right) \left(\frac{h}{0.73} \right) \left(\frac{1+z}{1.8} \right)^{1/2} \times \left(\frac{\Omega_m + \Omega_\Lambda (1+z)^{-3}}{0.37} \right)^{-1/2} \text{ mK} \quad (4)$$

The simulated 21cm fluctuation temperature map with $\delta T_{21}(\vec{x}) = b_{\text{HI}} \bar{T}_{21} \delta(\vec{x})$ is shown in the top panel of Fig. 2. We also produce a map convolved with a Gaussian beam whose FWHM resolution is 0.25° , corresponding to the resolution of a telescope with an aperture of ~ 100 m at 800 MHz frequency, this is shown in the bottom panel of Fig. 2.

We also include a few simple foreground models in the simulation. At the low frequencies, we consider three kinds of spectrum indices of diffuse foreground: the Galactic synchrotron emission which dominates the low-frequency sky; a slightly more sophisticated model with frequency-varying index; multiple indices which are likely to be produced by additional components such as synchrotron emission, free-free emission, etc. In the simplest case, the brightness temperature of the foreground component is modeled with a single spectral index,

$$f(\nu) = A_* \left(\frac{\nu}{\nu_*} \right)^{\beta_*} \quad (5)$$

We adopt $A_* = 5.3$ K, the average temperature of foreground at 800 MHz (Zheng et al. 2017), $\beta_* = -2.76$ (Reich & Reich 1988; Testori et al. 2001). A slight improvement is to consider a running index foreground given by Wang et al. (2006)

$$f(\nu) = A_* \left(\frac{\nu}{\nu_*} \right)^{\beta_* - 0.1 \ln(\nu/\nu_*)} \quad (6)$$

Finally, for multiple indices foreground

$$f(\nu) = 5.3 \left(\frac{\nu}{\nu_*} \right)^{-2.76} + 0.2 \left(\frac{\nu}{\nu_*} \right)^{-2.1} + 0.1 \left(\frac{\nu}{\nu_*} \right)^{-3.2} \quad (7)$$

In Fig. 3, we show the input 21cm signal along one line of sight in the top panel, and the total temperature including the 21cm signal, the foreground (a single power index component) and randomly generated noise in the bottom panel.

3. RESULTS

Here we apply this method to the extraction of 21cm signal from the observational data with foreground and

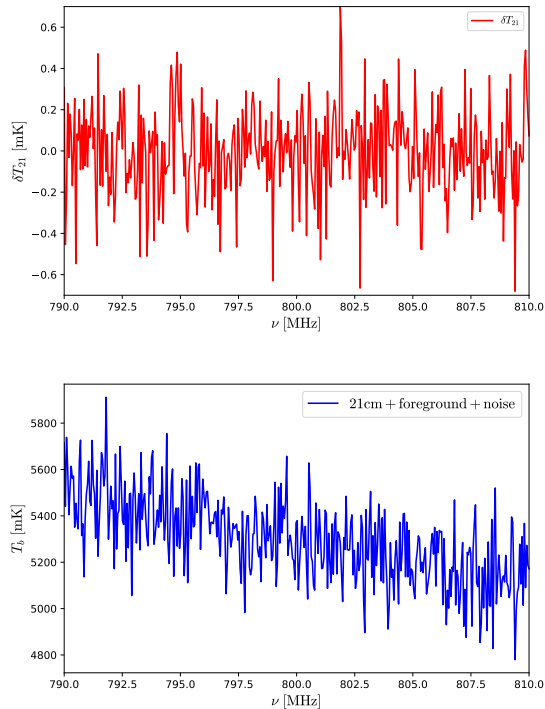


Figure 3. The input spectrum along one line of sight. Top: the input 21cm signal; Bottom: 21cm signal + single index foreground + noise.

noise. In the present paper, we shall adopt a two step procedure: in the first step, we process the data cube along each line of sight by removing the smoothly distributed foreground component. In the second step, we apply the Wiener filter in the two dimension angular space, which reduce the noise significantly to recover the 21cm signal.

3.1. Frequency Filtering

In frequency space, for the relatively low resolution (0.1 MHz) required for intensity mapping, we may neglect the small side lobes in the frequency channels, and take $\mathbf{A} = \mathbf{I}$, where \mathbf{I} is the identity matrix. We rewrite Eq. (1) as

$$y(\nu) = f(\nu) + s(\nu) + n(\nu) \quad (8)$$

where $f(\nu)$ is the foreground, $s(\nu)$ is the 21cm signal, $n(\nu)$ is the noise, which we assume to be a white noise with zero mean. We assume the signal, foreground and noises are uncorrelated with each other, so that $\langle (\mathbf{f} + \mathbf{s} + \mathbf{n})(\mathbf{f} + \mathbf{s} + \mathbf{n})^T \rangle = \mathbf{F} + \mathbf{S} + \mathbf{N}$, where $\mathbf{S} = \langle \mathbf{s}\mathbf{s}^T \rangle$, $\mathbf{F} = \langle \mathbf{f}\mathbf{f}^T \rangle$, and $\mathbf{N} = \langle \mathbf{n}\mathbf{n}^T \rangle$.

Along one line of sight, both the 21cm signal and the noise are stochastically varying on the relevant scales, while the foreground is more smooth, so here we may

use this to extract the foreground from the data first. If we ignore the slight imperfection in frequency channels which are fairly small, so that the response can be treated as δ function, the foreground extraction filter is given by $\mathbf{W}_\nu^f = \mathbf{F}(\mathbf{F} + \mathbf{S} + \mathbf{N})^{-1}$, while the signal+noise is given by $\mathbf{W}_\nu = \mathbf{I} - \mathbf{W}_\nu^f$.

We note that in the real world the foreground is unknown, so strictly speaking the Wiener filter method can not be applied. Nevertheless the foreground is believed to be smooth in the frequency space, so that even though the Wiener filter constructed this way is not very precise, it could still serve as a low-pass filter to extract the smooth component of the data. In fact, we also tried applying a simple low-pass filter and found the result is practically the same.

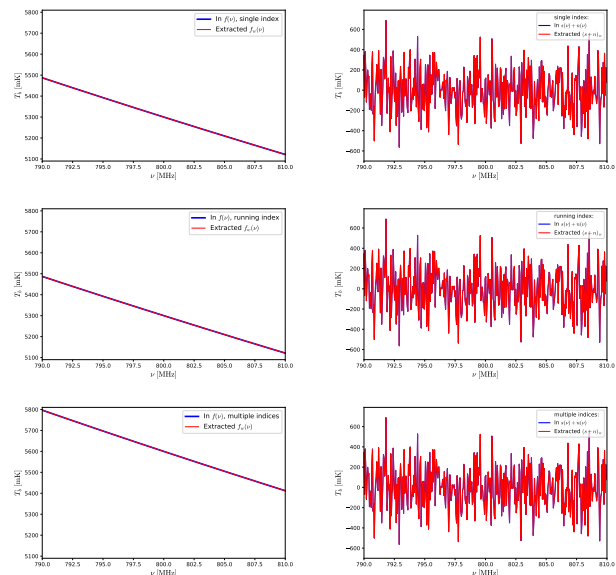


Figure 4. Left: extracted foregrounds ($\mathbf{W}^f \mathbf{y}$). Right: extracted 21cm+noise ($[\mathbf{I} - \mathbf{W}^f] \mathbf{y}$). Top to bottom: different foreground models with single index, running index and multiple indices respectively.

The filtered data $\mathbf{W}^f \mathbf{y}$ and $[\mathbf{I} - \mathbf{W}^f] \mathbf{y}$ are shown for a random line of sight in Fig. 4. From top to bottom, the three panels show the result for the single index, varying index and multi-component cases respectively. The smoothly varying and stochastically varying components are separated, but the 21cm signal is still mixed with the noise.

3.2. Angular Space Filtering

We make angular space filtering to separate the 21cm signal from the noise. To simplify the notation, we will omit the frequency variable ν in the expressions given below, though it should be understood that all the observables and beams are functions of ν .

We label the pixels of the sky with the angular position $\vec{\theta}$, then the Gaussian beam response \mathbf{A} is given by

$$A_{\vec{\theta}, \vec{\theta}'} = \frac{1}{\sqrt{2\pi}\sigma_\theta} e^{-|\vec{\theta}-\vec{\theta}'|^2/(2\sigma_\theta^2)} \quad (9)$$

The covariance matrix \mathbf{S} is given by the angular correlation function of the signal,

$$\mathbf{S}_{\vec{\theta}, \vec{\theta}'} = \langle T_{21}(\vec{\theta})T_{21}(\vec{\theta}') \rangle = C(|\vec{\theta}-\vec{\theta}'|) \quad (10)$$

Here we have assumed that the 21cm signal is statistically isotropic and homogeneous, i.e. the statistics does not depend on the position in the sky or the direction $\vec{\theta}-\vec{\theta}'$. Expanding in spherical harmonics,

$$T(\vec{\theta}) = \sum_{l,m} a_{l,m} Y_{l,m}(\vec{\theta}) \quad (11)$$

Substitute Eq. (11) into Eq. (10), and using the relation $\langle a_{l,m} a_{l',m'}^* \rangle = C_l \delta_{l,l'} \delta_{m,m'}$, we obtain

$$C(|\vec{\theta}-\vec{\theta}'|) = \sum_{l,m} C_l Y_{l,m}(\vec{\theta}) Y_{l,m}^*(\vec{\theta}') \quad (12)$$

Using the addition theorem for spherical harmonics,

$$\sum_{m=-l}^l Y_{l,m}(\vec{\theta}) Y_{l,m}^*(\vec{\theta}') = \frac{2l+1}{4\pi} P_l(\vec{\theta} \cdot \vec{\theta}')$$

where P_l is the Legendre polynomial of l -th order, and $\vec{\theta} \cdot \vec{\theta}' = \cos \theta$ where θ is used to denote the angle between the unit vectors $\vec{\theta}$ and $\vec{\theta}'$, we finally obtain

$$\mathbf{S}_{\vec{\theta}, \vec{\theta}'} = \sum_l \frac{2l+1}{4\pi} C_l P_l(\cos \theta) \quad (13)$$

The C_l can be computed from the power spectrum by considering its projection on a thin shell with bandwidth $\Delta\nu$ (Santos et al. 2005),

$$C_l(\nu) = \frac{2\Delta\nu^2}{\pi} \int k^2 dk P_{2l}(k, \nu) j_l^2[kr(\nu)] \quad (14)$$

In Fig. 5 we show the angular power spectrum C_l (top panel) and corresponding angular correlation function $C(\theta)$ (bottom) panel. The correlation between 21cm signal drops rapidly at $l \sim 10^2$ or degree scale.

The noise covariance matrix for pixels $\vec{\theta}, \vec{\theta}'$ is given by

$$\mathbf{N}_{\vec{\theta}, \vec{\theta}'} = N_0 \delta_{\vec{\theta}, \vec{\theta}'}, \quad (15)$$

where for simplicity we have assumed a constant noise N_0 . Note that in Eq. (1), if the vector \mathbf{x} denoted sky pixels while \mathbf{y} denotes time-ordered data, then the different elements of \mathbf{n} are data taken at different time and may be considered independent random samples, so the noise

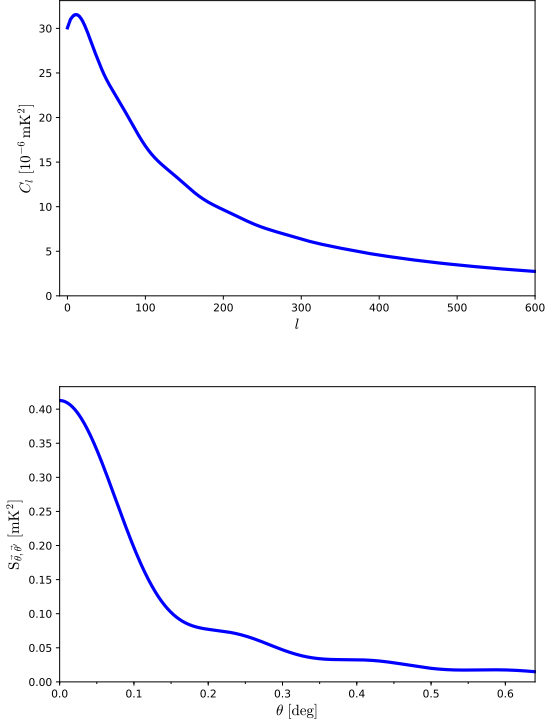


Figure 5. C_l (top) and $C(\theta)$ of 21cm signal at $z \sim 0.8$.

matrix \mathbf{N} is diagonal. If we use pixels finer than the beam size, then when we re-bin the time-ordered data into sky pixels, the noise in adjacent pixels with angular distance smaller than the beam size would be correlated, this is automatically taken into account in the Wiener filter Eq. (2) by the response matrix \mathbf{A} and \mathbf{A}^T . In the real world, the noise may be more complicated, for example, the noise level may be direction-dependent, either due to brighter sky temperature, or because the operating condition of the telescope receiver. Furthermore, even the data taken at different time may have some correlation due to the presence of $1/f$ noise. These effects can also be handled by the Wiener filtering algorithm, if the noise covariance matrix \mathbf{N} is known. In the present work we shall assume the simple case where the noise is uncorrelated and constant.

Fig. 9 shows the extracted 21 cm map by applying the Wiener filter. From top to bottom, we plot the input map with 21cm signal plus 200 mK noise, the extracted 21cm map, and the difference between the extracted map and the input map. Despite of the high noise level, the 21cm signal is successfully recovered, the difference between the recovered map and the original one is very small. Note that the Wiener filter is obtained by using the angular correlation function computed from the cosmological model, which corresponds to the ensemble

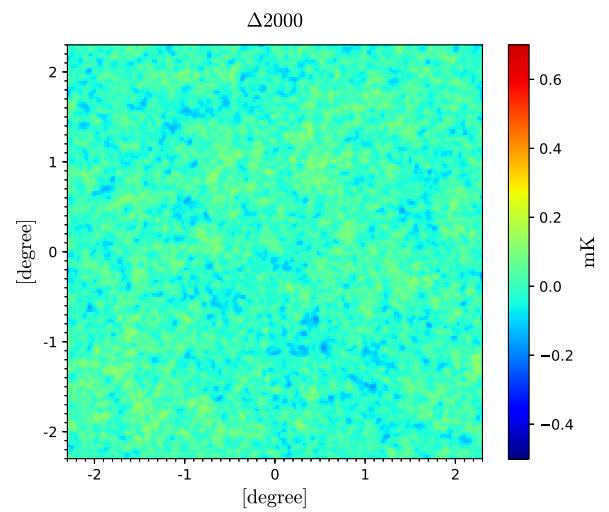
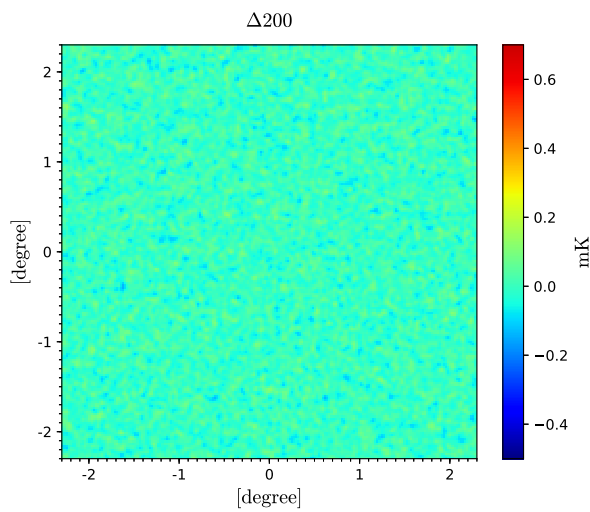
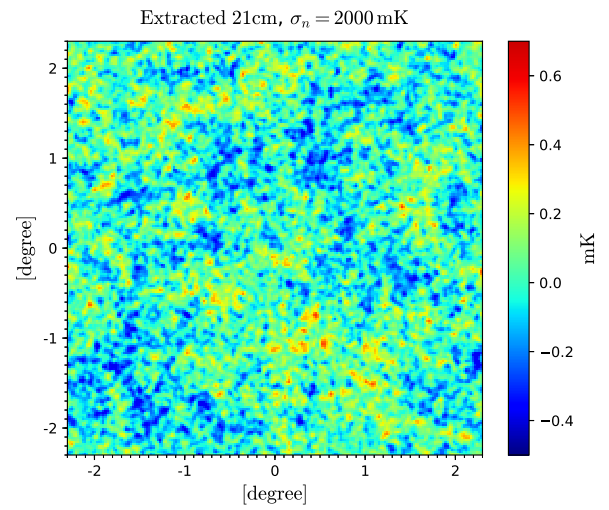
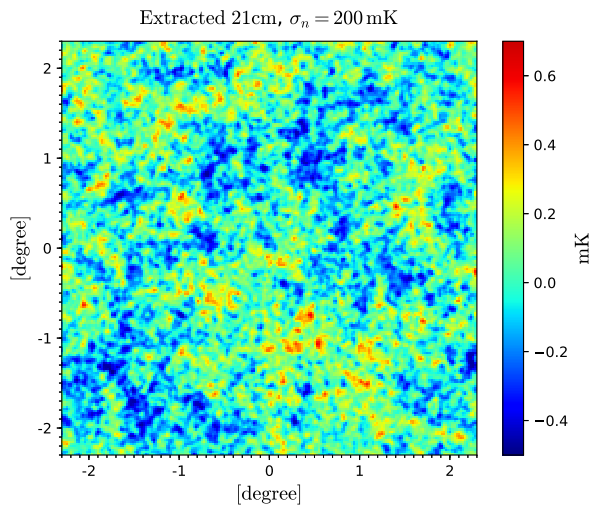
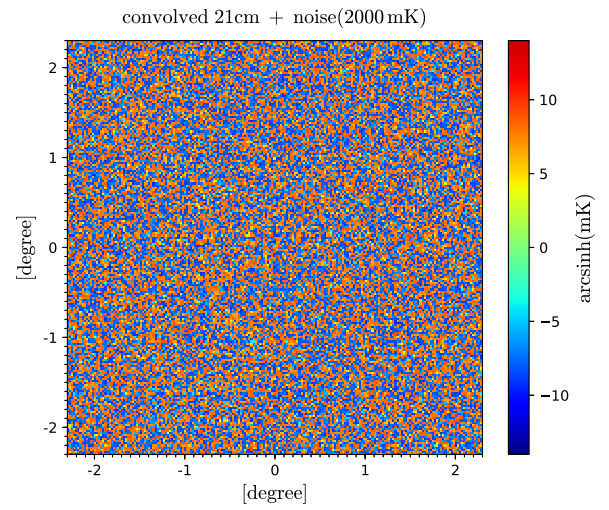
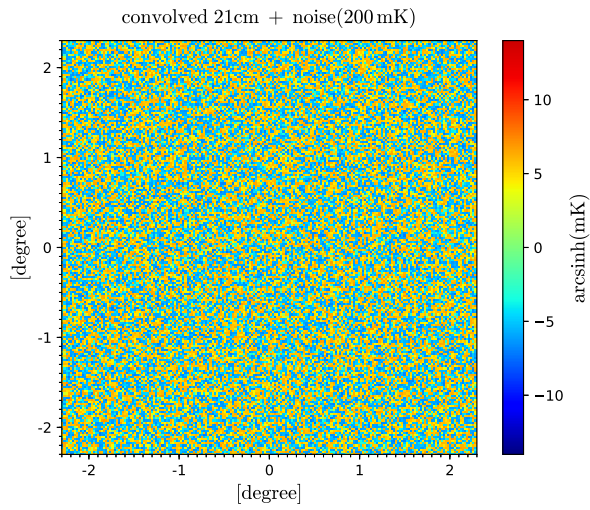


Figure 6. Top Panel: 21cm map + noise; Middle Panel: extracted 21cm map; Bottom: difference between the extracted and input 21cm maps.

Figure 7. Same as Fig. 9, but with higher noise level (2000 mK).

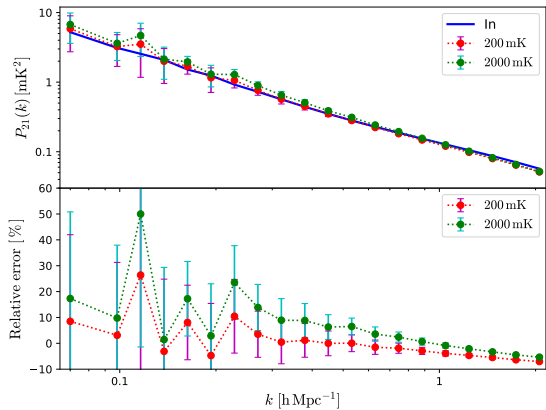


Figure 8. The recovered 21cm power spectrum (top panel) and the relative error (bottom panel) for this simulation box. We show the power for the original (blue line) signal, the reconstruction with 200 mK noise (red symbols), and 2000 mK noise (green symbols) in the figure.

average value, the actual realization may differ slightly due to sample variance, so the recovery would not be perfect.

In fact, the method could also work reasonably well even if the noise level is still higher. This is shown in Fig. 7, where the noise is assumed to be 2000 mK. Here we see that the difference between the recovered 21cm map and the original one is larger than in Fig. 9, but the overall structure of the 21cm intensity is still clearly seen, and the difference between the two maps is still much smaller than the 21cm brightness temperature.

In Fig. 8 we show the recovered 21cm power spectrum and the relative error. The error bars are estimated from the variance in k -space. The error obtained here is for the simulation box which is $(86 \text{ Mpc } h^{-1})^3$. If we assume that the relative error scales simply as $\Delta P/P \sim V^{-1/2}$, we estimate that in order to achieve 1% statistical precision on power spectrum at $k = 0.1 \text{ Mpc } h^{-1}$, the required survey volume is $(370 \text{ Mpc } h^{-1})^3$. The actual error may be larger when sampling variance and imperfection in reconstruction are taken into account.

When making the map, the Wiener filter automatically deconvolves the data. In the above analysis the beam is assumed to be perfectly known, so the recovery is very accurate even when noise is present. Indeed, some finer details whose scales are smaller than that of the beam width are recovered in the reconstructed map, which shows the power of the Wiener filter method. However, in the real world the beam is only known either by electromagnetic field simulation, or by calibration measurements, and both approaches have errors. We make a simple demonstration of the effect of inac-

curately known beam by the following exercise: we assume the real beam is an Gaussian with a beam width (FWHM) of 0.25° , but then in the reconstruction we use Gaussian beams with slightly different beam widths. The result is shown in Fig. 9. The top panels show the original 21cm signal (top left, same as the top panel of Fig. 2) and the reconstructed map with the correct beam size (top right, same as the middle panel of Fig. 9), we put these here again for easy comparison. The bottom panels show the reconstructed map with Gaussian beams of incorrect beam widths of 0.23° (Bottom Left) and 0.20° (Bottom Right). We see that when the incorrect beam widths are used, the whole reconstructed map become "fuzzier", the finer details of the original maps are lost, though the overall large scale structure are still very similar. In the real world, of course, the deviation from the beam might be more irregular and complicated, but the overall effect would be losing the details below the beam resolution while retaining the larger overall structures.

4. DISCUSSIONS AND CONCLUSION

A 3D cosmological neutral hydrogen survey over a large fraction of the sky is an efficient way to study our universe. A number of instruments have been developed or are being designed for such surveys. However, a great challenge is that both the foreground radiation and the noise are several orders of magnitude larger than the 21cm signal. To extract the cosmological 21cm signal from the data collected from such instruments, an efficient extraction method is required.

This paper is an exploratory study of this issue using the Wiener filter, which is widely utilized in signal processing field. We have taken as an example the analysis of data processing for a mid-redshift experiment, which is aimed at measuring the dark energy equation of state by using the BAO features in the large scale structure. However, the method is also applicable for the EoR experiments. Assuming that the data has been pre-processed, and an image cube have been produced, we used a two step procedure to extract the 21cm signal. We first subtract the foreground by removing the smooth component in the frequency spectrum along each line of sight. Previously, Liu & Tegmark (2012) applied the Wiener filter method to extract the foreground from 21cm experiment, but they are mostly concerned mostly with the frequency spectrum, which is applicable to 21cm global spectrum experiment, or to one line of sight for the 21cm intensity mapping experiment, corresponding to this first step. However, we then go one step further, extracting the 21cm signal by applying the Wiener filter on the two dimensional angular space. Our

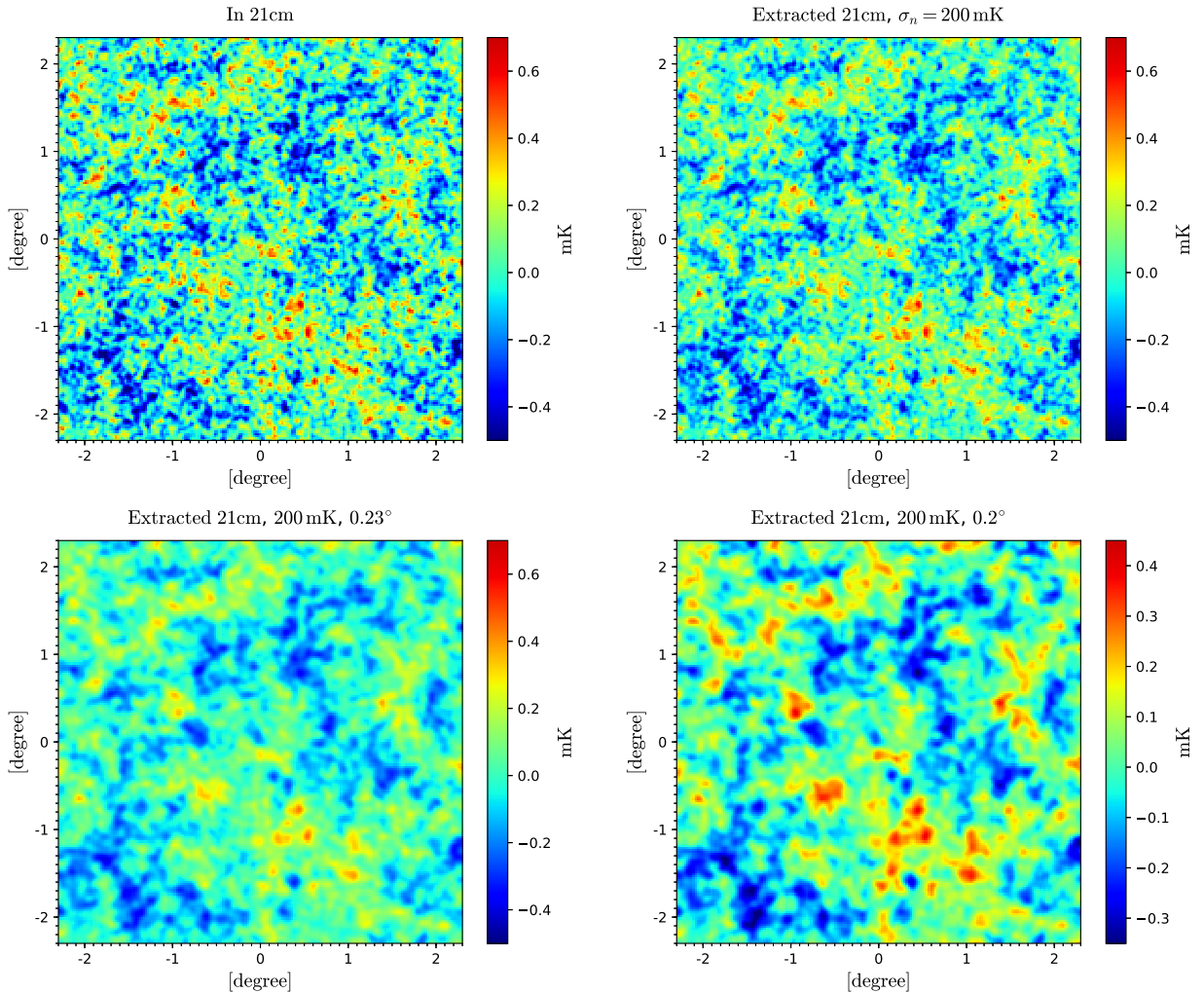


Figure 9. Effect of inaccurate beam on map reconstruction. We assume here the real beam size is 0.25° . Top Left: input 21cm map; Top Right: reconstructed 21cm map from noise of 200 mK, with the correct beam size of 0.25° ; Bottom Left: reconstruction with the incorrect beam width of 0.23° ; Bottom Right: reconstruction with the incorrect beam width of 0.20° .

simulation show that the 21cm signal could be recovered with good precision. In actual data analysis, the power spectrum of the 21cm signal is not precisely known, but from other cosmological observations approximate value could be inferred. Starting from an approximate value, one can apply the filter iteratively to improve the estimate.

In the present study we have made a number of simplifying assumptions. In an actual experiment, the beam shape is more complicated, frequency-dependent and only known to a limited precision, the calibration proce-

cedure may introduce additional errors, and the noise may be non-thermal and have more complicated statistical properties. All of these factors may affect the extraction of the 21cm signal. To overcome these problems, one needs to consider the specific experiment. Nevertheless, the Wiener filtering may provide a very useful tool for 21cm data analysis.

This research is supported by the Ministry of Science and Technology grant 2016YFE0100300, NSFC grants 11473044, U1501501, U1631118, 11633004, and CAS grant QYZDJ-SSW-SLH017. F. Q. Wu also acknowledge the support by the CSC Cai Yuanpei grant.

REFERENCES

- Bandura, K., Addison, G. E., Amiri, M., et al. 2014, in Proc. SPIE, Vol. 9145, Ground-based and Airborne Telescopes V, 914522
- Battye, R. A., Browne, I. W. A., Dickinson, C., et al. 2013, MNRAS, 434, 1239

- Chang, T.-C., Pen, U.-L., Bandura, K., & Peterson, J. B. 2010, *Nature*, 466, 463
- Chang, T.-C., Pen, U.-L., Peterson, J. B., & McDonald, P. 2008, *Physical Review Letters*, 100, 091303
- Chapman, E., Abdalla, F. B., Harker, G., et al. 2012, *MNRAS*, 423, 2518
- Chen, X. 2012, in *International Journal of Modern Physics Conference Series*, Vol. 12, *International Journal of Modern Physics Conference Series*, 256–263
- Ciardi, B., & Madau, P. 2003, *ApJ*, 596, 1
- de Oliveira-Costa, A., Tegmark, M., Gaensler, B. M., et al. 2008, *MNRAS*, 388, 247
- DeBoer, D. R., Parsons, A. R., Aguirre, J. E., et al. 2017, *PASP*, 129, 045001
- Dickinson, C. 2014, *ArXiv e-prints*, arXiv:1405.7936
- Gleser, L., Nusser, A., & Benson, A. J. 2008, *MNRAS*, 391, 383
- Huynh, M., & Lazio, J. 2013, *ArXiv e-prints*, arXiv:1311.4288
- Jelić, V., Zaroubi, S., Labropoulos, P., et al. 2008, *MNRAS*, 389, 1319
- Liu, A., & Tegmark, M. 2012, *MNRAS*, 419, 3491
- Loeb, A., & Zaldarriaga, M. 2004, *Phys. Rev. Lett.*, 92, 211301
- Madau, P., Meiksin, A., & Rees, M. J. 1997, *ApJ*, 475, 429
- Mao, Y., Tegmark, M., McQuinn, M., Zaldarriaga, M., & Zahn, O. 2008, *PhRvD*, 78, 023529
- Masui, K. W., Switzer, E. R., Banavar, N., et al. 2013, *ApJL*, 763, L20
- Nan, R., Li, D., Jin, C., et al. 2011, *International Journal of Modern Physics D*, 20, 989
- Newburgh, L. B., Bandura, K., Bucher, M. A., et al. 2016, *ArXiv e-prints*, arXiv:1607.02059
- Paciga, G., Chang, T.-C., Gupta, Y., et al. 2011, *MNRAS*, 413, 1174
- Parsons, A. R., Backer, D. C., Foster, G. S., et al. 2010, *AJ*, 139, 1468
- Planck Collaboration, Ade, P. A. R., Aghanim, N., et al. 2016, *A&A*, 594, A13
- Reich, P., & Reich, W. 1988, *A&AS*, 74, 7
- Santos, M. G., Cooray, A., & Knox, L. 2005, *ApJ*, 625, 575
- Santos, M. G., Cooray, A., & Knox, L. 2005, *Astrophys. J.*, 625, 575
- Shaver, P. A., Windhorst, R. A., Madau, P., & de Bruyn, A. G. 1999, *A&A*, 345, 380
- Switzer, E. R., Masui, K. W., Bandura, K., et al. 2013, *MNRAS*, 434, L46
- Tegmark, M. 1997, *Astrophys. J.*, 480, L87
- Testori, J. C., Reich, P., Bava, J. A., et al. 2001, *A&A*, 368, 1123
- Tingay, S. J., Goeke, R., Bowman, J. D., et al. 2013, *PASA*, 30, 7
- van Haarlem, M. P., Wise, M. W., Gunst, A. W., et al. 2013, *A&A*, 556, A2
- Wang, X., Tegmark, M., Santos, M. G., & Knox, L. 2006, *ApJ*, 650, 529
- Wolz, L., Abdalla, F. B., Blake, C., et al. 2014, *MNRAS*, 441, 3271
- Xu, Y., Wang, X., & Chen, X. 2015, *Astrophys. J.*, 798, 40
- Zhang, J., Ansari, R., Chen, X., et al. 2016a, *Mon. Not. Roy. Astron. Soc.*, 461, 1950
- Zhang, J., Zuo, S., Ansari, R., et al. 2016b, *Res. Astron. Astrophys.*, 16, 158
- Zheng, H., Tegmark, M., Dillon, J. S., et al. 2017, *MNRAS*, 464, 3486
- Zheng, Q., Wu, X.-P., Johnston-Hollitt, M., Gu, J.-h., & Xu, H. 2016, *ApJ*, 832, 190
- Zuo, S., Chen, X., Ansari, R., & Lu, Y. 2018, *ArXiv:1801.04082*